PCCP

Accepted Manuscript

ROYAL SOCIETY OF CHEMISTRY

www.rsc.org/pccp

Journal Name

ARTICLE TYPE

Cite this: DOI: 10.1039/xxxxxxxxxx

Brownian motion of a nano-colloidal particle: The role of the solvent

Alexis Torres-Carbajal,[a] Salvador Herrera-Velarde,[b,c] and Ramón Castañeda-Priego[c]

Received Date
Accepted Date

DOI: 10.1039/xxxxxxxxxx

www.rsc.org/journalname

Brownian motion is a feature of colloidal particles immersed in a liquid-like environment. Usually, it can be described by means of the generalised Langevin equation (GLE) within the framework of the Mori theory. In principle, all quantities that appear in the GLE can be calculated from the molecular information of the whole system, i.e., colloids and solvent molecules. In this work, by means of extensive Molecular Dynamics simulations, we study the effects of the microscopic details and the thermodynamic state of the solvent on the movement of a single nano-colloid. In particular, we consider a two-dimensional model system in which the mass and size of the colloid are two and one orders of magnitude, respectively, larger than the ones associated with the solvent molecules. The latter ones interact via a Lennard-Jones-type potential to tune the nature of the solvent, i.e., it can be either repulsive or attractive. We choose the linear momentum of the Brownian particle as the observable of interest in order to fully describe the Brownian motion within the Mori framework. We particularly focus on the colloid diffusion at different solvent densities and two temperature regimes: high and low (near the critical point) temperatures. To reach our goal, we have rewritten the GLE as a second kind Volterra integral in order to compute the memory kernel in real space. With this kernel, we evaluate the momentum-fluctuating force correlation function, which is of particular relevance since it allows us to establish when the stationarity condition has been reached. Our findings show that even at high temperatures, the details of the attractive interaction potential among solvent molecules induce important changes on the colloid dynamics. Additionally, near to the critical point, the dynamical scenario becomes more complex; all the correlation functions decay slowly in an extended time window, however, the memory kernel seems to be only a function of the solvent density. Thus, the explicit inclusion of the solvent in the description of Brownian motion allows us to better understand the behaviour of the memory kernel at those thermodynamic states near the critical region without any further approximation. This information is useful to elaborate more realistic descriptions of Brownian motion that take into account the particular details of the host medium.

1 Introduction

Since the seminal work of Ludwig E. Boltzmann for the description of the molecular motion of gases [1], several theoretical frameworks have been proposed to determine the transport properties of atomic liquids [2–11] and macro-molecules immersed in a continuum medium [12,13]. The main goal of such approximations is to formulate hydrodynamic equations that govern the dynamical properties of a system by taking into account its molecular features. These theoretical formalisms are commonly built through two different but equivalent routes: (1) the method of the distribution functions and (2) the formalism of the correlation functions. The former method allows us to derive equations of the type: Fokker-Planck [14] and Smoluchowski [12] equations, whereas the latter expresses the transport coefficients in terms of the change in time of state variables. However, the main disadvantage of the aforementioned routes resides in the fact that, at least, an additional approximation is needed to solve the set of equations. This approximation is not derived from first principles and, therefore, the limit of applicability where the solution holds is typically narrow.

On the other hand, the so-called Molecular Dynamics (MD) simulation technique has been successfully employed to describe the thermodynamic properties of systems composed of either

[a]*División de Ciencias e Ingenierías, Campus León, Universidad de Guanajuato, Loma del Bosque 103, Lomas del Campestre, 37150 León, Guanajuato, Mexico*
[b]*Subdirección de Postgrado e Investigación, Instituto Tecnológico Superior de Xalapa, Sección 5A Reserva Territorial s/n, 91096, Xalapa, Veracruz, Mexico*
[c]*Departamento de Ingeniería Física, División de Ciencias e Ingenierías, Campus León, Universidad de Guanajuato, Loma del Bosque 103, Lomas del Campestre, 37150 León, Guanajuato, Mexico; Tel: 52 477 7885100; E-mail: ramoncp@fisica.ugto.mx*

atoms or macromolecules, and even stars, that interact each other through a given potential[15]. Therefore, MD simulations can be used to compute, for instance, the correlation functions that describe entirely the dynamical properties of many-body systems. For example, MD simulations have already been employed to determine the friction coefficient, ξ, of a system made up of a colloidal particle of infinite mass immersed in both hard-sphere[16] and Lennard-Jones[17] solvents. However, colloids have a finite mass and are much bigger than the solvent molecules. In fact, a current challenge for any simulation technique is to deal with systems whose components exhibit very large size and mass asymmetries, e.g., colloids immersed in an explicit solvent. Nowadays, due to the enormous increase in the speed of the computer processors together with advanced numerical methods that allow us to optimise MD algorithms, one can study systems with moderate size and mass asymmetries[18]. Thus, it is possible to fully describe the *Brownian motion* in the nano-colloidal regime.

One of the main characteristics of a colloid immersed in an aqueous environment is the so-called Brownian motion. The theoretical description of the Brownian motion by the pioneering work of Einstein[13] and Smoluchowski[12] established the bases for the understanding of the transport of macromolecules in a suspension[19]. The description of the Brownian motion by Langevin[20] is based on the fact that there exist essentially two forces acting on a single colloid: thermal forces induced through collisions with the solvent molecules, typically referred to as thermal noise and modelled as Gaussian noise, and the friction force originated by the solvent viscosity, which damps the particle motion. In such description, the solvent is considered as a continuum medium characterised by a constant viscosity, however, its nature and thermodynamics are not taken into account explicitly. Nevertheless, in an effort to incorporate the microscopic details of the solvent within the Langevin description, Deutch and Oppenheim employed the projection operator technique to describe the Brownian motion of a single heavy particle[21] and several heavy particles[22] immersed in a bath of N light particles. From computational point of view, recent advances on the Brownian motion with the explicit inclusion of the solvent are related with systems composed of a colloid of finite mass and size in a repulsive LJ solvent[23,24], with particular interest in the calculation of both diffusion[23] and friction[24] coefficients.

Mori has suggested deviations in the so-called generalised Langevin equation (GLE) that arise from the molecular information of the solvent, which includes memory effects[25]. Mori formalism is directly based on the calculation of correlation functions, however, they cannot always be easily computed[26]. Nevertheless, in the particular case of the Brownian motion of a single heavy particle of mass M interacting with a large number of solvent particles of mass m, a Markovian description can be done in the limit $m/M \to 0$[27].

In a system where several species with widely different characteristic time and space scales coexist, it is almost impossible to take into account all the degrees of freedom and it is a common practice to resort to a coarse grained description integrating from the description, i.e., from either the equations of motion or the partition function, all degrees of freedom that do not belong to the main larger constituent. This leads to a state dependent effective description for the main constituent, thereby allowing a one-component model description (for example, the standard Langevin equation of motion for the colloids only). The motivation for such a procedure is not only to facilitate contact with experiments, where most of the time the small constituents cannot be probed directly, but also to simplify the theoretical treatment. However, in the particular case of a colloidal dispersion, the solvent details, i.e., the interaction potential among solvent molecules and the thermodynamic state, are of considerable importance because recent studies have shown that a Langevin approach cannot longer be applied since the thermal motion due to the collisions with the solvent deviates from the classical Gaussian noise picture[28,29]. Additionally, Pesce et al. experimentally measured the effects of fluid inertia on the diffusion of a Brownian particle at very long time scales[30]; their experimental data are consistent with a generalised theory that takes into account not only the inertia contribution of the colloidal particle, but also the inertia of the solvent molecules. Furthermore, interesting phenomena, such as the critical Casimir forces[31] and the colloidal self-assembly near critical solvents[32] cannot be fully understood if the role of the solvent on the static and dynamical properties of colloidal dispersions is not studied in detail. Therefore, the explicit inclusion of the solvent becomes relevant to understand the underlying mechanisms that lead to such phenomena.

Hence, the aim of this work is to study the Brownian motion of a single nano-colloid immersed in an explicit solvent. In particular, we focus on the effects caused by both the nature and thermodynamic state of the solvent. More specifically, we are mainly interested in the following question: *what is the role of a solvent that exhibits a gas-liquid coexistence on the diffusion of a nano-colloid?* Then, from the molecular information, we evaluate all the correlation functions needed to fully describe the diffusion of the colloidal particle. The memory kernel is thus computed and analysed in order to highlight the influence of the solvent on the particle dynamics.

After the previous Introduction, the manuscript is organised as follows. In section 2, we present the generalised Langevin equation in the framework of the Mori theory and the expressions to calculate the memory and the fluctuating force autocorrelation functions are shown. In section 3, we briefly describe the microscopic details of the system under study and provide the main characteristics of the MD simulations carried out in this contribution. The results for the momentum autocorrelation function, memory kernel and momentum-fluctuating force correlation of the nano-colloid in terms of the thermodynamic state of the solvent are presented in section 4, including those near the critical point. Finally, we summarise our main findings in the section of concluding remarks.

2 Description of Brownian motion from the molecular dynamics and the Generalised Langevin equation

Mori theory describes the Brownian motion in terms of correlation functions, such as the momentum autocorrelation,

momentum-force and total force autocorrelation functions[25]. These functions allow one to compute the so-called memory kernel, as it is explained further below, and to fully describe the features of the Brownian motion. Furthermore, within the Mori framework, the change of a given variable is determined by two contributions; one of them called systematic, which is composed of an instantaneous and a retarded contribution, and the second one is random. The retarded contribution is determined by the memory kernel and is associated with the momentum autocorrelation function through the dissipation-fluctuation theorem[33].

Let us choose the linear momentum $\mathbf{P}$ of the Brownian particle as the variable of interest and assume a system free of external fields. Then, the generalised Langevin equation can be written as[17,25,34],

$$\dot{\mathbf{P}}(t) = -\int_0^t ds \mathbf{k}(t-s)\mathbf{P}(s) + \mathbf{F}^+(t), \tag{1}$$

where $\mathbf{F}^+$ is the fluctuating force with mean value $\langle \mathbf{F}^+ \rangle = 0$, with $\langle \cdot \rangle$ denoting an ensemble average, $\mathbf{k}$ is the memory kernel and $t-s$ is related to the correlation time. According to the dissipation-fluctuation theorem, the components of the fluctuating force are related with the memory kernel through the expression[33]

$$\langle F_\alpha^+(t) F_\beta^+(s) \rangle = \sum_\gamma \langle P_\alpha P_\beta \rangle k_{\gamma,\beta}(t-s), \tag{2}$$

where α, β, γ denote the cartesian components: x, y, z. Due to the isotropy of the microscopic model, the previous equation reduces to the following set of equations,

$$\langle F_\alpha^+(t) F_\beta^+(s) \rangle = \delta_{\alpha\beta} \langle \mathbf{F}^+(t) \mathbf{F}^+(s) \rangle, \tag{3}$$

$$\langle P_\alpha P_\beta \rangle = \frac{\delta_{\alpha\beta}}{3} \langle P^2 \rangle, \tag{4}$$

$$k_{\alpha,\beta}(t-s) = \delta_{\alpha\beta} k(t-s). \tag{5}$$

Then, one can write the relation between the Cartesian components of the fluctuating force and the memory kernel as follows,

$$\langle F^+(t) F^+(s) \rangle = \langle P^2 \rangle k(t-s). \tag{6}$$

Every component of the force must satisfy the same scalar generalised Langevin equation, i.e.,

$$\dot{P}(t) = -\int_0^t ds\, k(t-s) P(s) + F^+(t), \tag{7}$$

and F^+ obeys the scalar fluctuation-dissipation theorem given by eq. (6).

By multiplying eq. (7) with $P(0)$ and taking the ensemble average, one obtains

$$\begin{aligned} \langle \dot{P}(t) P(0) \rangle &= -\int_0^t ds\, k(t-s) \langle P(s) P(0) \rangle \\ &\quad + \langle F^+(t) P(0) \rangle. \end{aligned} \tag{8}$$

Let us now define the momentum autocorrelation function as $C(t) \equiv \langle P(t) P(0) \rangle$. Then, by considering that the fluctuating force $F^+(t)$ and the momentum $P(0)$ are statistically independent, one can rewrite eq. (8) as an equation of motion for the momentum autocorrelation function

$$\dot{C}(t) = -\int_0^t ds\, k(t-s) C(s). \tag{9}$$

2.1 Memory kernel from molecular dynamics simulations

In a MD simulation, one has full access to the microscopic information, like the particle position, momentum and total force at every instant. In fact, with a MD simulation, one can compute directly the momentum autocorrelation function, nevertheless, it is not possible to determine the random contribution to the total force in this way. As one can observe in eq. (9), it is possible to determine the memory function from this relation and use eq. (6) to calculate the random contribution.

Usually, from eq. (9), a Laplace transform is performed in order to calculate the memory function, however, this procedure can bring errors due to the numerical stability implied in the Laplace transformation[35,36]. In general, eq. (9) describes a first kind Volterra equation[37] for the memory kernel. However, every integral of first kind Volterra equation can be rewritten as a second kind Volterra equation by taking the derivate with respect to the independent variable. In this case, one obtains the following expression,

$$\ddot{C}(t) = -C(0) k(t) - \int_0^t ds\, \dot{C}(t-s) k(s). \tag{10}$$

It is possible to numerically calculate $\ddot{C}(t)$ and $\dot{C}(t)$, but one should avoid the numerical differentiation considering that such functions can be expressed as the total force autocorrelation and the momentum total force correlation functions, respectively,

$$\ddot{C}(t) = -\langle F(t) F(0) \rangle, \tag{11}$$

$$\dot{C}(t) = \langle F(t) P(0) \rangle, \tag{12}$$

Then, the correlation function can be determined directly from the MD simulation. Thus, the GLE (see eq. (9)) can be reexpressed as,

$$\langle F(t) F(0) \rangle = C(0) k(t) + \int_0^t ds\, \langle F(t-s) P(0) \rangle k(s). \tag{13}$$

There are different proposals to solve a Volterra integral equation of second kind[38–40], nevertheless, one does not have to forget that in this case the memory kernel is unknown. According to the estimation of the correlation functions, one knows its value at every Δt, so one can use this information to apply a very standard discretisation procedure. With the discretisation of eq. (13), one immediately gets

$$\begin{aligned} \langle F(i\Delta t) F(0) \rangle &= C(0) k(i\Delta t) + \\ &\quad \Delta t \sum_{j=0}^{i} w_j \langle F(i\Delta t - j\Delta t) P(0) \rangle k(j\Delta t), \end{aligned} \tag{14}$$

where $w_j = 1/2$ for $j = 0, i$, and $w_j = 1$ in other case, represents the integration weight factor. Then, $k(t)$ at each $t = i\Delta t$ can be

computed in an iterative way as,

$$k(i\Delta t) = [C(0)+\Delta t w_i \langle FP\rangle]^{-1}\times \left[\langle F(i\Delta t)F(0)\rangle - \Delta t\sum_{j=0}^{i-1} w_j \langle F((i-j)\Delta t)P(0)\rangle k(j\Delta t)\right], \quad (15)$$

with the initial condition $k(0)=\langle F^2\rangle/C(0)$. Thus, by means of MD simulations, the memory kernel can be straightforwardly computed.

In this contribution, we systematically study the memory kernel of a single nano-colloidal particle as a function of the thermodynamic state of the solvent.

2.2 Stationarity

A MD simulation begins with a specification of initial conditions, where neither the bath nor the Brownian particle are in thermodynamic equilibrium. Even if the initial conditions can be such that the system is near the equilibrium state, it is necessary to run the simulation a long enough time until the equilibrium state has been established. In order not to choose a particular initial state, in the GLE the initial state is shifted to the infinitely remote past[34] , i.e.,

$$\dot{P}(t) = -\int_{-\infty}^{t} ds\, k(t-s)P(s) + F^{+}(t). \quad (16)$$

Hence, to be consistent with the Mori formulation (7), one has to keep the relation (9) between the memory kernel $k(t)$ and the momentum autocorrelation function. Then, the fluctuating force and the momentum are correlated as follows

$$\langle P(0)F^{+}(t)\rangle = \int_{0}^{\infty} ds\, k(t+s)C(s). \quad (17)$$

In contrast with Mori formalism[25], where the initial momentum and the fluctuating force at positive times are uncorrelated, as we early mentioned, the stationarity in the simulation requests a correlation between these quantities. Moreover, one can show that the stationary Langevin equation in conjunction with relation (17) implies the fluctuation-dissipation theorem. For the fluctuating force, one can write

$$F^{+}(t) = \dot{P}(t) + \int_{-\infty}^{t} ds\, k(t-s)P(s), \quad (18)$$

where the force $F(t)$ gives the acceleration of the Brownian particle, i.e., $F(t)=\dot{P}(t)$. By multiplying eq. (18) with $P(0)$ and performing an equilibrium ensemble average, one finds

$$\langle P(0)F^{+}(t)\rangle = \dot{C}(t) + \int_{0}^{t} ds\, k(t-s)C(s) + \int_{-\infty}^{0} ds\, k(t-s)C(s). \quad (19)$$

According to eq. (9), the first two terms in eq. (19) cancel each other and only the third term remains. Changing the variable of integration $s\to -s$ and considering the symmetry of the correlation function $\langle P(0)P(t)\rangle \equiv C(t)=C(-t)$, one immediately obtains the expression of the fluctuating force momentum correlation (17). Thus, from MD simulations one can extract the set of correlations functions that allow us to fully understand the nature of the Brownian motion.

3 Microscopic model

We consider a $2D$ system made up of N soft discs of mass m and diameter σ_{fl} that form the solvent and a single Brownian particle of mass M and diameter σ_B. The Hamiltonian of the colloid-solvent system is given by[22,24,34]

$$H = \frac{1}{2M}\mathbf{P}^2 + \sum_{i=1}^{N}\frac{1}{2m}\mathbf{p}_i^2 + \sum_{i}^{N} U_B(|\mathbf{r}_i-\mathbf{R}|) + \sum_{i\neq j}^{N} U_{fl}(|\mathbf{r}_i-\mathbf{r}_j|), \quad (20)$$

where $\mathbf{r}_i$ and $\mathbf{R}$ are the solvent particle and Brownian particle positions, respectively. Similarly, $\mathbf{p}_i$ and $\mathbf{P}$ are the linear momenta, respectively. The solvent-Brownian inter-particle potential is given by the potential U_B, which in this work is expressed by the so-called WCA potential (introduced further below). The solvent-solvent interaction is given by the potential U_{fl} with the functional form of a WCA potential for the repulsive solvent and a Lennard-Jones potential for the attractive solvent.

Hauge and Martin Löf[41] pointed out that a necessary condition to observe Brownian motion, i.e., a stochastic-like motion, is described by the ratio $\gamma \equiv \left(\frac{\rho_{fl}}{\rho_B}\right)^{1/2} \ll 1$, where ρ_{fl} and ρ_B are the mass densities of the solvent and the Brownian particles, respectively. However, Lebowitz [27,42] and Zwanzig[43] found that an appropriate criterium to establish Brownian motion is given by the condition $\gamma' \equiv \left(\frac{m}{M}\right)^{1/2} \ll 1$. Both conditions, γ and γ', are equivalent if one considers the mass of the Brownian particle, M, as the main physical parameter to be varied. In this work, we particularly consider a Brownian particle of mass, $M=100m$, so $\gamma'=0.1$. Hence, strictly speaking, we are not working in the limit previously mentioned, but, this chosen value for γ' is close to the one for nano-colloids immersed, for example, in benzene[44].

The MD simulations are carried out in the NVT ensemble with a system composed of $N=15000$ solvent discs and a single Brownian disc. The discs are initially distributed on a surface in a square array as initial particle configuration with random velocities that satisfy the equipartition theorem; this allows us to reach the thermal equilibrium much faster. In the MD simulations, we have used the so-called iso-kinetics thermostat, i.e., a simple rescaling of the particle velocities. To improve the statistics, we have averaged all the correlation functions over 10 different initial seeds, i.e., different initial points in the phase space. This method allows the system to follow different paths in the phase space. However, it is important to point out that we are dealing with one single nano-colloid and, therefore, the statistical uncertainties associated to any physical observable are not negligible. Clearly, the ideal scenario is to have many colloids in the very dilute regime to avoid colloid-colloid interactions to get a better statistics. Unfortunately, from computational point of view, this case cannot be reached in a realistic time because increasing the number of nano-colloids leads to a considerable increase, of several orders of mag-

nitude, in the number of solvent molecules. Thus, a simulation with a larger number of colloids with the explicit incorporation of the solvent molecules is currently a challenging task. The statistical uncertainties associated to each correlation function were obtained according to the procedure described in Ref.[45].

The reduced units of length, temperature and time are defined as $r^* \equiv r/\sigma_{fl}$, $T^* \equiv k_B T/\varepsilon$ and $t^* \equiv t/\tau$, respectively, where the time unit is $\tau = \sigma_{fl}\sqrt{m/\varepsilon}$, with k_B and T being the Boltzmann's constant and the absolute temperature, respectively, and ε is defined further below. The reduced density is defined as $\rho^* = 4\eta/\pi$, where η is the solvent packing fraction $\eta = N\pi\sigma_{fl}^2/4A$, i.e., the ratio between the area occupied by the solvent discs and the total available area, A.

The equations of motion are integrated with the standard velocity Verlet algorithm[45], employing a time step $\Delta t = 1\times10^{-3}\tau$ to guarantee its stability. In all cases, we have done 5×10^6 integration steps to establish thermal equilibrium. From the subsequent 3×10^7 time steps, we compute the observables to fully reconstruct the generalised Langevin equation.

To better understand the effect of the thermodynamic state of the solvent on the Brownian motion, as first scenario we consider a purely repulsive solvent with a temperature $T^* = 1.0$; this state is particularly defined as the high temperature regime, and two solvent densities, namely, $\rho^* = 0.40, 0.80$. In a second case, we study the effects of an attractive solvent on the dynamical behaviour of the Brownian particle. In this case, the dynamics is studied near the saturated regions; close to the vapour and liquid branches, and in the neighbourhood of the solvent critical point.

The gas-liquid phase diagram of the attractive solvent is here computed by means of Monte Carlo computer simulations in the Gibbs ensemble (GEMC)[46–48]. For the construction of the phase diagram, we consider a system of $N = 1000$ solvent discs randomly distributed in two square surfaces of area A. In both surfaces, we impose periodic boundary conditions. The thermalisation of the system is reached with 9×10^7 Monte Carlo (MC) steps and 9×10^8 additional steps are employed to compute the liquid and vapour coexistence densities. The maximum particle displacement and the volume change ratio are adjusted to obtain 30% and 50% of acceptation ratios, respectively.

As mentioned in the previous paragraph, the determination of the gas-liquid coexistence is carried out by means of GEMC simulations. However, a few points of the binodal reported in Fig. 3 (see below) were also corroborated with our MD simulation technique (data not shown) using the so-called canonical method[49]. Thus, we are confident that the MD simulations are reproducing the actual dynamics of the system.

3.1 Repulsive solvent

During the study of Brownian motion, the solvent is typically treated implicitly[50,51], however, recent investigations show that the thermodynamic state of the solvent plays an important role in explaining new emergent phenomena, such as the critical Casimir forces[52–55]. Hence, in this work we deal with the explicit incorporation of the solvent to systematically study the dynamics of a nano-colloidal particle. As a first case of study, we consider a repulsive solvent, i.e., a system whose molecules interact only via repulsive forces. The intermolecular interaction between the solvent discs is given by the so-called WCA potential[56]

$$u_{WCA}(r) = \left\{4\varepsilon\left[\left(\frac{\sigma_{fl}}{r}\right)^{12} - \left(\frac{\sigma_{fl}}{r}\right)^{6}\right] + \varepsilon\right\}\Theta(r - r_c), \qquad (21)$$

where ε is the interaction strength between discs. Θ is the Heaviside function, r is the inter-molecular separation and r_c is the cut-off radius. The WCA potential contains only repulsive interactions, see dashed line in Fig. 1. Inset of Fig. 2 shows that the structural behaviour of this solvent is basically independent of the reduced temperature, T^*. This solvent and its role in the Brownian motion of a single particle has already been studied by Shin *et al.*[34]. In such contribution, authors studied the Brownian motion for various characteristics of the Brownian particle. However, due to the repulsive nature between molecules, this system only undergoes liquid and solid phases[57]. Then, in such system the colloid dynamics near the liquid-vapor transition could not be studied.

3.2 Attractive solvent

The interaction potential among discs of the attractive solvent is given by the Lennard-Jones potential[58,59]. This potential has been subject of extensive investigations[60–62]. The main reason resides in its simple functional form that allows one to model attractive interactions of relative short-range. It has been shown that the optimal LJ potential to be used in a molecular dynamics simulation should be truncated at the cut-off radius, r_c, and shifted to be zero at longer inter-particle separations; this procedure avoids the discontinuity of the force due the truncation and the inclusion of the so-called long-tail corrections[63]. The differences between both LJ and WCA potentials are shown in Fig. 1. The potential $u_{LJ}(r)$ has the following functional form,

$$u_{LJ}(r) = [\phi(r) - \phi(r_c)]\,\Theta(r - r_c), \qquad (22)$$

where the function $\phi(r)$ is the standard LJ potential,

$$\phi(r) = 4\varepsilon\left[\left(\frac{\sigma_{fl}}{r}\right)^{12} - \left(\frac{\sigma_{fl}}{r}\right)^{6}\right], \qquad (23)$$

We identify eq. (22) as the Lennard-Jones spherical truncated and shifted (LJ-STS) potential.

As it is well-known, the short-range attractive interaction confers to the solvent a richer structural and thermodynamic behaviour than the one observed in a solvent with repulsive interactions. One can verify this statement directly from Fig. 2, where the radial distribution function, $g(r)$, for both solvents at the same reduced density for different temperatures is explicitly shown; main body displays the $g(r)$ of the attractive solvent and inset shows the corresponding one of the repulsive solvent. There, one can notice that the microscopic structure of the attractive solvent depends strongly on the temperature, however, as expected, in the high temperature regime, the behaviour of both solvents is very similar. In fact, the potential (21) was originally proposed to investigate the influence of repulsive interactions on the structure of LJ-like solvents[56], i.e., simple liquids. However, when the

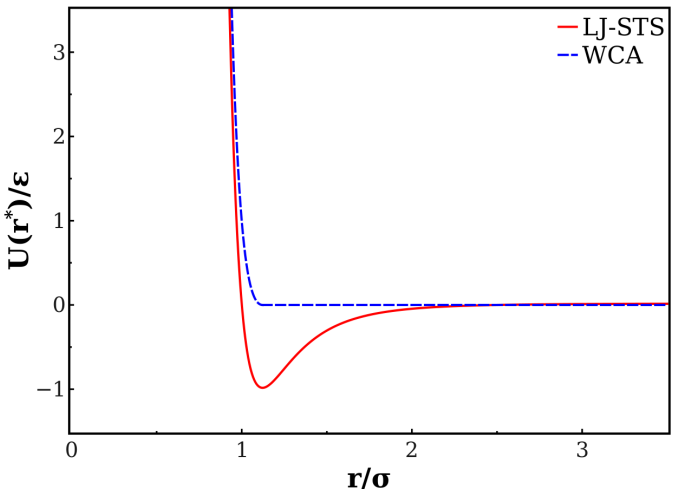

Fig. 1 WCA (dashed line) and LJ (continuos line) potentials for the interaction between repulsive and attractive, respectively, solvent molecules. The repulsive potential is given by eq. (21) and the attractive one by eq. (23) shifted and truncated at $r_c = 2.5\sigma$.

temperature decreases, the system becomes more structured and, particularly, the second maximum of the $g(r)$ exhibits a split, see Fig. 2 for $T^* = 0.4$; this structural behaviour is typically associated to a liquid-solid transition[64].

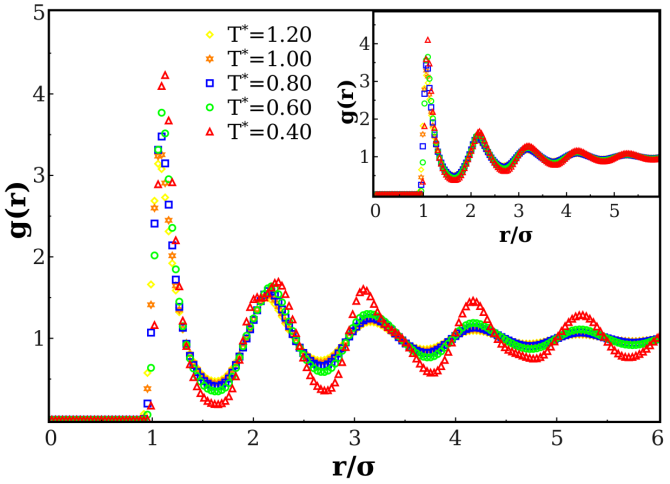

Fig. 2 Radial distribution function, $g(r)$, for various reduced temperatures at the reduced density $\rho^* = 0.80$ of the attractive solvent (23). At $T^* = 0.40$, the second maximum shows a dislocation; this characteristic indicates a solid-liquid phase transition. Inset shows the radial distribution functions for the same reduced density and temperatures for the repulsive solvent (21).

In order to make a systematic study along several isotherms close to the binodal, we also calculate the phase diagram of the LJ potential (22). The results of the GEMC simulations are shown in Fig. 3. The critical point is estimated by using a scaling law and the law of rectilinear diameters[65]. According to this procedure, the critical point parameters, ρ_c and T_c, are fitting parameters of the following equations

$$\rho_l^* - \rho_v^* = C_1 \left(T_c^* - T^*\right)^\beta , \tag{24}$$

$$\frac{\rho_l^* + \rho_v^*}{2} = \rho_c^* + C_2 \left(T_c^* - T^*\right), \tag{25}$$

where ρ_l^* and ρ_v^* are the reduced coexistence densities of liquid and vapour, respectively, at the reduced temperature T^*. The critical exponent used is $\beta = 1/8$[66], with C_1 and C_2 being fitting parameters. Thus, our estimation for the critical point is $\rho_c^* = 0.36 \pm 0.01$ and $T_c^* = 0.451 \pm 0.003$.

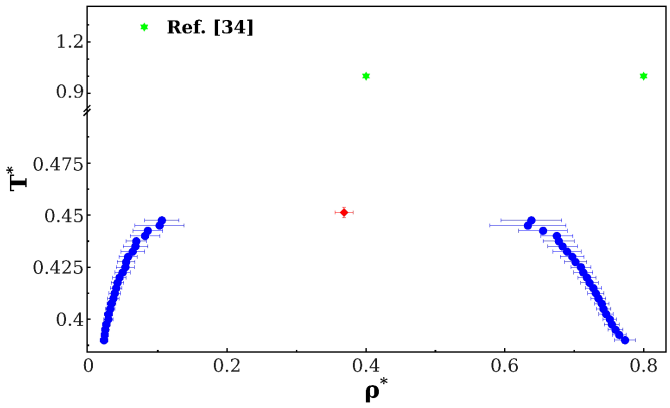

Fig. 3 Phase diagram of the attractive solvent given by eq. (22) with a cut-off radius $r_c = 2.5\sigma$. The circles are the orthobaric densities calculated by the GEMC simulation technique. The diamond is the critical point at $(\rho_c^*, T_c^*) = (0.36 \pm 0.01, 0.451 \pm 0.003)$ obtained by fitting the simulation data with eqs. (24) and (25). The stars are thermodynamic states for the repulsive solvent at the high temperature regime; this system has also been studied by Shin *et al.*[34] (see eq. (21)).

4 Results and discussion

The numerical evaluation of any correlation function, particularly at long times, is a technical problem of great difficulty[67]. Therefore, to reduce the statistical uncertainties, all the correlation functions are averaged over a large time window (two orders of magnitude greater than the one reported in the plots). Additionally, we have run the simulations in a sufficiently large box in order to avoid strong fluctuations of the correlation functions at long times. Such fluctuations are typically associated to the sound wave generated by the nano-colloidal particle, *i.e.,* the motion of the nano-colloid generates a perturbation in the solvent, which propagates across the simulation box and could influence the motion of the nano-colloids placed in the image boxes[68]. Then, in order to reduce these fluctuations, the simulation domain must be large, so the time it takes the sound wave to traverse the simulation area does not affect the determination of the correlation functions used, for example, to compute the memory kernel. In particular, we tested several box sizes, ranging from $N = 1000$ to $N = 15000$, and found that the largest one allowed us to reduce drastically this effect. We collect the simulation data every third time step $\Delta t = 3 \times 10^{-3}\tau$.

We firstly focus on two solvent densities at a high temperature and analyse the way in which the nature of the interaction potential between solvent molecules affects the dynamical behaviour of the nano-colloid. Secondly, we explore the dynamical changes of the nano-colloid when the thermodynamic state of the attractive

solvent is near to its critical point.

4.1 High temperature regime

4.1.1 Momentum autocorrelation function

The momentum autocorrelation function, $C(t)$, for a Brownian particle of diameter σ_B and mass $M = 100m$ immersed in a solvent at the temperature $T^* = 1.0$ for two different solvent concentrations is shown in Fig. 4. We have particularly chosen those thermodynamic states indicated by a star in the phase diagram of Fig. 3, which correspond to densities higher than the critical concentration in the high temperature domain. For comparison purposes, Fig. 4 also includes simulation results for the repulsive case studied by Shin et al.[34].

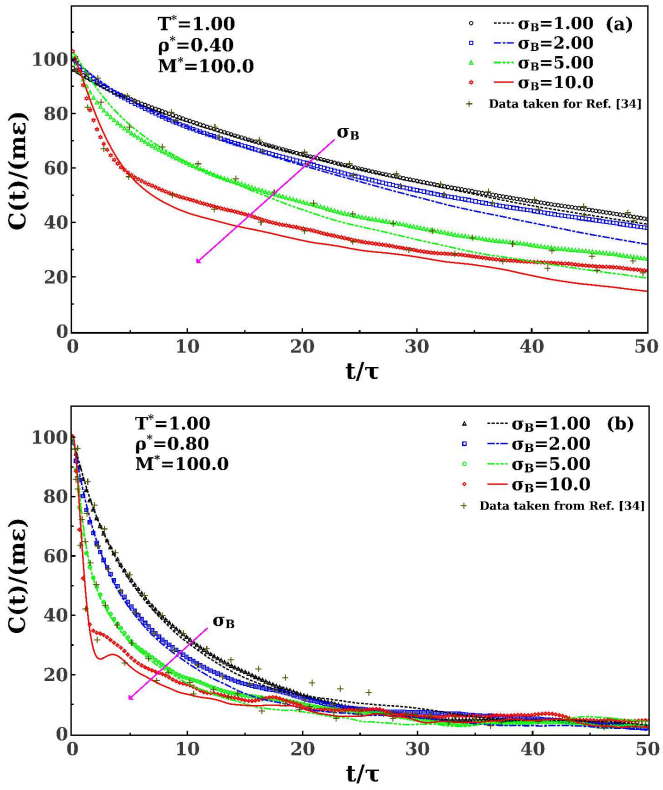

Fig. 4 Momentum autocorrelation function, $C(t)$, of a Brownian particle of mass $M = 100m$ immersed in a solvent with a particle concentration of (a) $\rho^* = 0.4$ and (b) $\rho^* = 0.8$ at the reduced temperature $T^* = 1.0$. These state points correspond to the stars indicated in Fig. 3 above the critical density. The direction of increase of the Brownian particle size is indicated with the arrow. The symbols and lines denote the cases for the repulsive and attractive solvents, respectively. Crosses denote the simulation results for the pure repulsive solvent reported by Shin et al.[34].

In this regime, $C(t)$ has a similar qualitative behaviour for both repulsive and attractive solvents, although small variations are noticed. This similarity is related with the fact that at high temperatures the repulsion among solvent discs dominates and the solvent structure is only a function of the density, see Fig. 2. It is also evident that at low and moderate solvent concentrations, for example, $\rho^* = 0.4$ (see Fig. 4a), the function displays a monotonic and slower decay due to the Brownian particle has a larger mean free path, in contrast with a higher solvent density, $\rho^* = 0.8$, where $C(t)$ exhibits a much faster decay (see Fig. 4b). In all cases, our simulation results for the repulsive case is in excellent agreement with the ones reported by Shin et al.[34].

From Fig. 4, it is evident that the amplitude of the correlation for the attractive solvent is slightly higher at short times, whereas at longer times there appears a crossover and the amplitude becomes now lower; this is more notorious at moderate concentrations and the time at which such crossover occurs decrease when the size of the Brownian particle increases. This behaviour might be associated with the heterogeneous distribution of solvent discs around the Brownian one due to the (weak) attraction among the former ones. This mechanism produces voids, i.e., the empty areas, of variable size and shape where the colloid is moving[69]. Thus, the results point toward that the attraction among solvent discs induces a heterogeneous distribution of voids that favour the momentum correlation at short-times, i.e., within the time window at which the colloid moves inside a void, but make difficult the colloid diffusion at longer times.

Additionally, one can observe that at high densities and high size asymmetries, $C(t)$ exhibits an oscillating decay behaviour. This feature might be associated with the following combined facts. On one hand, at high concentrations the medium becomes highly structured due to the enhancement of the inter-particle collision rate (this mechanism favours the association among solvent molecules) and, therefore, the colloid should diffuse in a strong correlated network, see Fig. 2. On the other hand, when the colloid is much bigger than the solvent molecules, the former spends much more time inside the (huge) cage created by the latter ones. Then, the process of colloidal diffusion should happen in regular leaps, i.e., when the colloid is able of escaping from the cage[69].

4.1.2 Memory kernel

We now turn our discussion to the effects of the solvent on the behaviour of the memory kernel. Again, for comparison purposes, simulation results for the repulsive case studied by Shin et al.[34] are explicitly included in the plot. As one can see in Fig. 5, the memory kernel depends strongly on the nature of the solvent. In fact, unlike $C(t)$, where the qualitative behaviour is similar in both types of solvents, the memory kernel exhibits clear differences associated to the intrinsic features of the solvent. This means that $k(t)$ is more sensitive to the details or functional form of the intermolecular potential between solvent discs. Furthermore, it decays much faster than the momentum autocorrelation function (see Fig. 4).

The memory kernel, $k(t)$, decays in the same fashion for all sizes of the Brownian particle, although at short times its amplitude in the case of the repulsive solvent is greater than that of the attractive one. However, the opposite trend is observed at long times. Another interesting characteristic observed in the memory kernel for the case of the attractive solvent is seen when the size of the Brownian particle increases, its decay becomes slower and the $k(0)$ value decreases monotonically as compared with the case of the repulsive solvent. This behaviour is more evident at lower solvent densities. Additionally, at higher solvent densities the magnitude of the memory kernel increases but its form is un-

affected. Again, our simulation results for the repulsive solvent are in good agreement with the ones presented by Shin et al.[34].

To better understand the features discussed in the previous paragraph, one should take a look at equation (15). Therefore, the decrease in the amplitude and the slower decay when increasing the Brownian particle size in the case of the attractive solvent is strongly connected with the enhancement of the momentum-force correlation contribution due to the attractive forces between solvent molecules, as compared with the repulsive case, which seems to be highly dominated by the momentum autocorrelation contribution due to the (possible) dominance of the repulsive forces. Hence, the degree of association of the solvent molecules (even at high temperatures) clearly affects the dynamics of the Brownian particle.

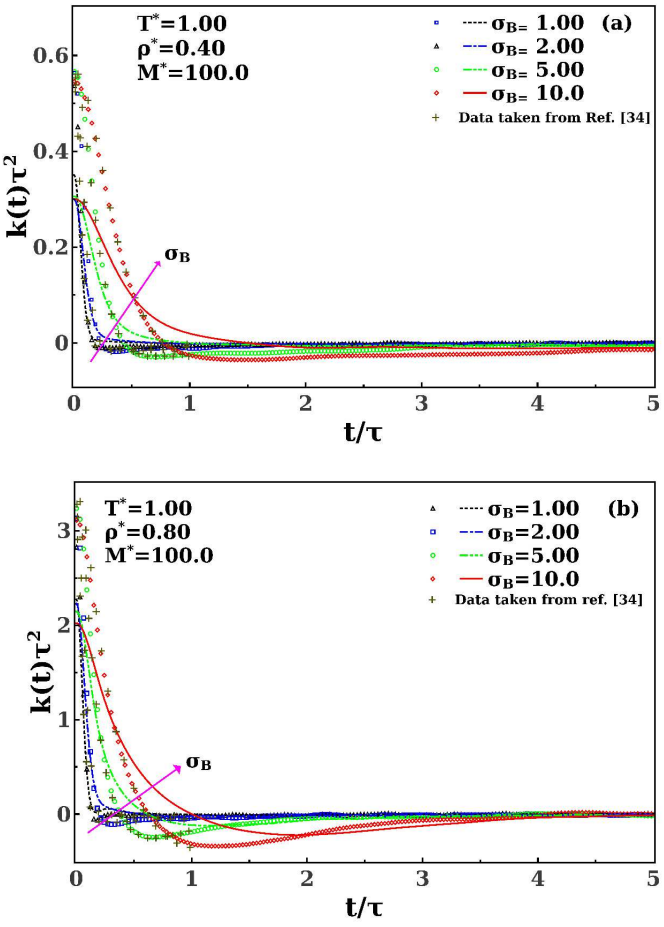

Fig. 5 The memory kernel $k(t)$ of the Brownian particle for the same scenarios displayed in Fig. 4.

4.1.3 Momentum-fluctuating force correlation function

The stationary momentum-fluctuating force correlation function, from now on denoted as $\langle P(0)F^{+}(t)\rangle$, is calculated by means of Eq. (17) and its behaviour at high temperatures for solvent concentrations above the critical one is depicted in Fig. 6. As can be seen from the figure, the correlation function has mainly negative values, except at very short-times where it is positive. This means that the momentum and the stochastic force are anti-correlated, i.e., they act in opposite directions, excluding the short-times where they act cooperatively.

The correlation $\langle P(0)F^{+}(t)\rangle$ depends on the product of the memory kernel and the momentum autocorrelation function (see Eq. 17). Thus, it possesses features that are clearly a combination of both functions. In particular, one notices that its magnitude becomes more negative when the diameter of the Brownian particle increases and goes to zero faster when the solvent density increases. In the case of the attractive solvent, it is less anti-correlated, however, its decay is slower. In both solvents, when the size of the Brownian particle is equal to the size of the solvent molecules, it goes to zero very quickly. Interestingly, the position of its minimum is a function of the details of the interaction potential among solvent molecules and the size ratio, but not of the solvent concentration.

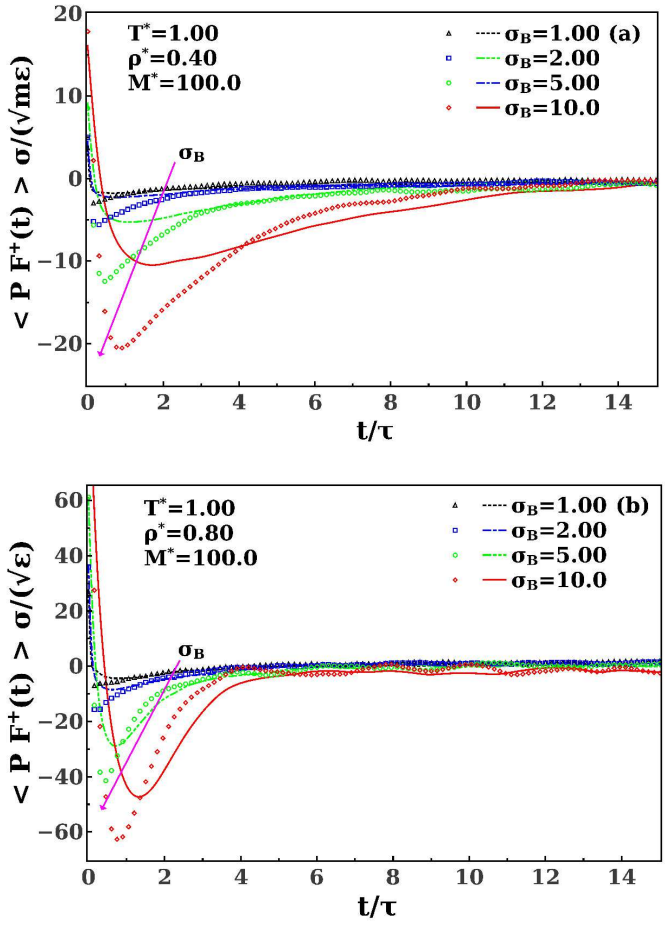

Fig. 6 Momentum-fluctuating force correlation function calculated from Eq. (17) of the Brownian particle for the same scenarios displayed in Fig. 4.

4.2 Critical Regime

So far we have studied the effects that the solvent has on the dynamics of a single nano-colloid when the interaction potential between solvent molecules is characterised mainly by either a repulsion or an attraction. We have also pointed out the way in which the solvent concentration and the size ratio among the Brownian

particle and a solvent molecule both affect the colloidal diffusion. We have particularly investigated the region of high temperatures and even there we observed that a small attraction among the solvent molecules can modify drastically the dynamical behaviour of a colloidal particle.

Now, in order to study the influence of the thermodynamic state of the attractive solvent on the dynamics of the Brownian particle, we focus on the colloidal dynamics in the neighbourhood of the critical point of the solvent (see Fig. 3). We particularly consider three solvent concentrations, namely, $\rho^* = 0.045$ (gas phase), $\rho^* = \rho_c^* = 0.36$ (critical density) and $\rho^* = 0.70$ (liquid phase) at temperatures close to the critical one $T_c^* = 0.451$. In what follows, only results for the attractive solvent with $\sigma_B = 10\sigma_{fl}$ and $M = 100m$ are shown. Figure 7 displays characteristic configurations of the system under study at those densities referred above close to the critical temperature. Clearly, the distribution of solvent molecules around the nano-colloid are different; this behaviour indicates that the collision rate between the solvent discs and the nano-colloid is a function of the thermodynamic state of the system.

4.2.1 Momentum autocorrelation function

We first analyse the changes in the momentum autocorrelation function due to temperature variations at the critical density, ρ_c^*, see Fig. 8(a). To better understand the results, Fig. 7(b) shows a snapshots of the system where one can see that the solvent discs around the nano-colloid are not uniformly distributed. As can be observed from figure Fig. 8(a), $C(t)$ exhibits a slow decay in all the temperatures explored. Nonetheless, its decay is not a monotonous function of the temperature; this behaviour is related with the strong density fluctuations of the solvent that lead to a wide spectrum of long-range correlation lengths when the system is near to the critical region. When the temperature increases, the correlation function approaches to the behaviour seen in the high temperature regime previously discussed.

We now discuss the changes in $C(t)$ due to density variations at the reduced temperature, $T^* = 0.456$ (slightly above the critical temperature as can be seen in Fig. 3), see Fig. 8(b). In the vapour and critical regions, the behaviour of $C(t)$ is quite similar, although its decay is the main feature that differentiates both regions, being lower in the vapour phase due to the longer mean-free path of the colloid because the low collision rate among the solvent molecule and the Brownian particle, see Fig. 7(a). In fact, for times $t > 250\tau$ the correlation function still oscillates around zero (data not shown). This means that at thermodynamic states below the critical density and close to the critical temperature, the momentum relaxation of the Brownian disc occurs in a extended window of time. On the other hand, in the liquid branch of the solvent, the correlation function goes to zero quickly due to the increase of the inter-particle collisions. Thus, the momentum relaxation of the colloid within the liquid region of the host medium is reached much faster in good agreement with the original Langevin approach, which assumes that it occurs at times $t \geq \tau_B = M/\xi$ [17].

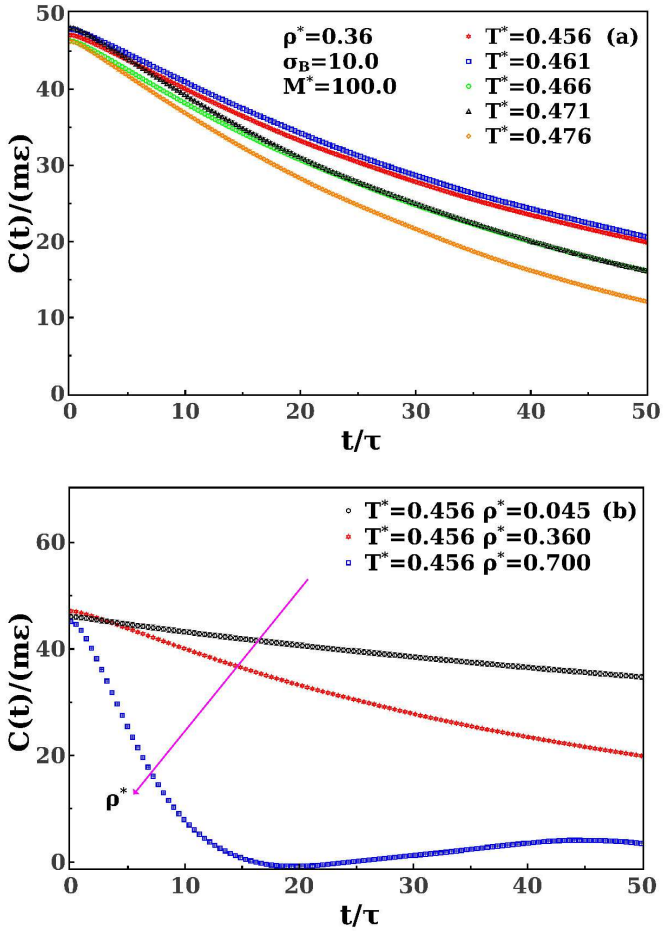

Fig. 8 Momentum autocorrelation function, $C(t)$, of a Brownian particle of mass $M = 100m$ and diameter $\sigma_B = 10\sigma_{fl}$ in various thermodynamic states of the solvent. In (a) the solvent density is $\rho^* = 0.36$ (the critical value) at several temperatures slightly above the critical temperature. In (b) a comparison between the behaviour of $C(t)$, in the vapor, critical and liquid densities of the solvent at the temperature $T^* = 0.456$.

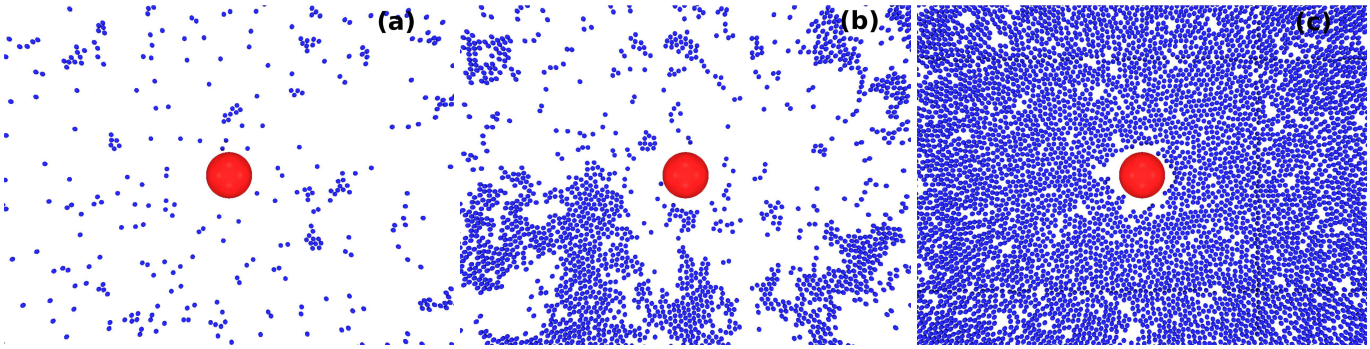

Fig. 7 Configurations of the system composed of a nano-colloid (big sphere) and an attractive solvent (small spheres) at different thermodynamic states. In panel (a) the solvent is in the gas phase $\rho^* = 0.045$, in panel (b) the solvent is in its critical density $\rho^* = \rho_c^* = 0.36$ and in panel (c) the solvent is in the liquid phase $\rho^* = 0.7$. In all cases, the reduced temperature is $T^* = 0.456$, just above the critical value (see Fig. 3). The mass and the diameter of the nano-colloid are $M = 100m$ and $\sigma_B = 10\sigma_{fl}$, respectively.

4.2.2 Memory kernel

The results for the memory kernel in the critical regime, for the same thermodynamics conditions reported in Fig. 8, are shown in Fig. 9. As it can be noticed, the memory kernel is a soft function of the thermodynamic state of the attractive solvent, whose magnitude does not change dramatically with the temperature, see Fig. 9a, but it does with the density, see Fig. 9b. In fact, inset of Fig. 9a shows that the memory kernel collapses onto a master curve when it is normalised with its value at $t = 0$. This behaviour indicates that $k(t)$ is a function of the density only. Below the critical density, its decay is relative fast, contrary to its slower decay at higher densities.

4.2.3 Momentum-fluctuating force correlation

The momentum-fluctuating force of the Brownian particle is displayed in Fig. 10. Along the isobaric points, we observe an interesting behaviour, see Fig. 10a. For the nearest temperature to the critical one, $T^* = 0.456$, the correlation function does not exhibit the anti-correlation mechanism observed in the high temperature regime, see Fig. 6, and it is purely cooperative. This means that both the momentum and the stochastic force act in the same direction at all times. To fully understand this behaviour, it is then necessary to study in more detail the underlying (microscopic) mechanisms that induce this kind of cooperativeness near the critical point. Furthermore, above such temperature, the correlation function becomes anti-cooperative at intermediate- and long-times, but, more interesting, it follows a similar quantitive dependence, suggesting that in such vicinity the momentum-fluctuating force correlation is not a function of the temperature. Of course, this is a property that holds in a narrow window of temperatures close to the critical one. Below the critical density, along the isotherm $T^* = 0.456$ (see Fig. 10b) the correlation function keeps its cooperative behaviour, however, it changes when the density increases and becomes highly correlated, i.e., its magnitude increases notably with the density.

Finally, we should stress that the dynamics of the Brownian particle seems to be more sensitive to the variations of the density rather than the changes in the temperature when it is close to the vicinity of the critical point.

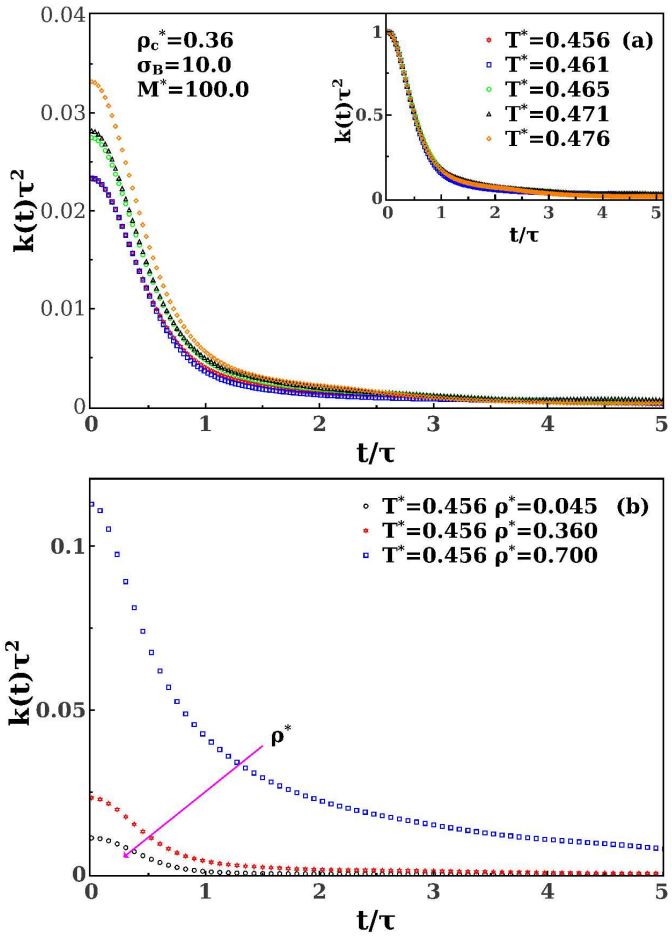

Fig. 9 Memory kernel, $k(t)$ of a Brownian particle of mass $M = 100m$ and diameter $\sigma_B = 10\sigma_{fl}$ for the same thermodynamic states reported in Fig. 8.

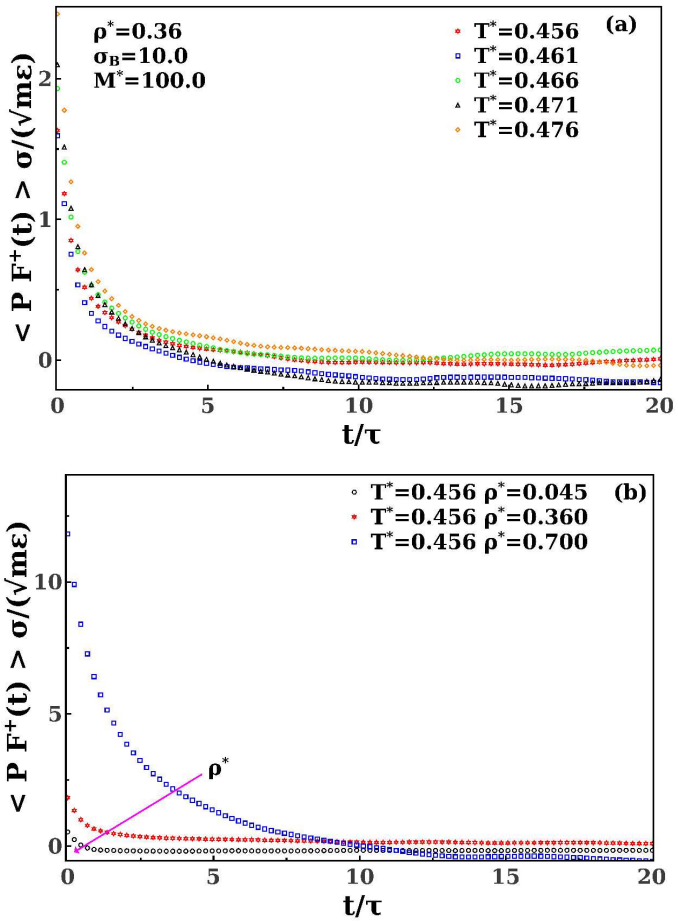

Fig. 10 Momentum-fluctuating force correlation function of a Brownian particle of mass $M = 100m$ and diameter $\sigma_B = 10\sigma_{fl}$ for the same the thermodynamic states reported in Fig. 8.

5 Concluding remarks

We reported on an extensive molecular dynamics study of the Brownian motion of a single nano-colloid immersed in a model solvent. We mainly focused on the effects on the colloid dynamics due to the nature of the solvent and its thermodynamic state. Then, by means of the molecular information, the Brownian motion was generated and analysed in terms of the generalised Langevin equation within the framework of the Mori theory.

In particular, the memory kernel was computed directly from the momentum autocorrelation function and the total force autocorrelation. We avoided the reference to a particular initial state inside the simulation, so the momentum-fluctuating force correlation is not null and its value was estimated from the memory kernel.

We also studied the momentum autocorrelation function for various diameters of the nano-colloid for two solvents of different nature, namely, repulsive and attractive, at different thermodynamic states; at high temperatures and near to the critical point. At high temperatures and large sizes of the nano-colloid, the shape of the momentum autocorrelation function was very similar in both solvents and such shape seemed to depend on the solvent concentration only. This behaviour was also confirmed around the critical temperature. At lower temperatures, particularly in the case of the attractive solvent and in the vicinity of the critical point, we found evidence of cooperativeness in the momentum-fluctuating force correlation function at long-times. Finally, the memory kernel of the Brownian particle allowed us to distinguish the effects associated to the interaction between solvent molecules and those linked to the thermodynamic state of the whole system. However, it is important to point out that the colloid dynamics became a function of the solvent concentration in the neighbourhood of the critical point.

Last, but not least, we should stress that in this work we employed potentials that historically have been used to model simple liquids. However, it would be very interesting to explore the colloidal dynamics by using those coarse-grained potentials that are able to capture the thermodynamic anomalies of real substances, such as the water[70]. Additionally, the effects of the (explicit) solvent on the correlation of a few colloidal particles, for example, colloids trapped in optical tweezers[71,72], is of great interest in order to better understand the hydrodynamic correlations in few-body systems. Work along these lines is in progress.

Acknowledgments

Authors acknowledge partial financial support from Conacyt (Grants Nos. 237425 and 375518). Authors also thank to the General Coordination of Information and Communications Technologies (CGSTIC) at Cinvestav for providing HPC resources on the Hybrid Cluster Supercomputer "Xiuhcoatl" that have contributed to the research results reported within this paper. R. C-P. also acknowledges the financial support provided by the Marcos Moshinsky fellowship 2013 - 2014.

References

1 S. R. de Groot and P. Mazur, *Non-equilibrium Thermodynamics*, Dover Publications, 1984.
2 J. G. Kirkwood, *J. Chem. Phys.*, 1946, **14**, 180–201.
3 J. G. Kirkwood, *J. Chem. Phys.*, 1947, **15**, 72–76.
4 J. G. Kirkwood, F. P. Buff and M. S. Green, *J. Chem. Phys.*, 1949, **17**, 988–994.
5 J. H. Irving and R. W. Zwanzig, *J. Chem. Phys.*, 1951, **19**, 1173–1180.
6 R. W. Zwanzig, J. G. Kirkwood, K. F. Stripp and I. Oppenheim, *J. Chem. Phys.*, 1953, **21**, 2050–2055.
7 R. W. Zwanzig, J. G. Kirkwood, I. Oppenheim and B. J. Alder, *J. Chem. Phys.*, 1954, **22**, 783–790.
8 J. Ross and J. G. Kirkwood, *J. Chem. Phys.*, 1954, **22**, 1094–1103.
9 J. Ross, *J. Chem. Phys.*, 1956, **24**, 375–380.
10 M. S. Green, *J. Chem. Phys.*, 1952, **20**, 1281–1295.
11 M. S. Green, *J. Chem. Phys.*, 1954, **22**, 398–413.
12 M. Smoluchowski, *Ann. Phys.*, 1906, **21**, 757–779.
13 A. Einstein, *Ann. Phys.*, 1906, **19**, 371–381.
14 H. Risken, *The Fokker-Planck Equation: Methods of Solution and Applications*, Springer, 1984.
15 M. P. Allen and D. J. Tildesley, *Computer Simulation of Liquids*, Claredon Press, 1991.
16 J. J. Brey and J. G. Ordóñez, *J. Chem. Phys.*, 1982, **76**, 216101.
17 P. Español and I. Zuñiga, *J. Chem. Phys.*, 1992, **98**, 574–580.
18 O. Awile, F. Büyükkececi, S. Reboux and I. F. Sbalzarini, *Computer Physics Communications*, 2012, **183**, 1073–1081.
19 S. Chandrasekhar, *Rev. Mod. Phys.*, 1943, **15**, 1–89.
20 P. Langevin, *C. R. Acad. Sci.*, 1908, **146**, 530–533.
21 J. Albers, J. M. Deutch and I. Oppenheim, *J. Chem. Phys.*, 1971, **54**, 3541–3546.
22 J. M. Deutch and I. Oppenheim, *J. Chem. Phys.*, 1971, **54**, 3547–3555.
23 D. Chakraborty, *Eur. Phys. J. B*, 2011, **83**, 375–380.
24 Song Hi Lee, *Theor. Chem. Acc.*, 2010, **127**, 613–619.
25 H. Mori, *Phys. Rev.*, 1958, **112**, 1829–1842.
26 H. Spohn, *Rev. Mod. Phys.*, 1980, **53**, 569–615.
27 J. L. Lebowitz and E. Rubin, *Phys. Rev.*, 1963, **131**, 2381–2396.
28 T. Franosch, M. Grimm, M. Belushkin, F. M. Mor, G. Foffi, L. Forró and S. Jeney, *Nature*, 2011, **478**, 85–88.
29 H. K. Shin, B. Choi, P. Talkner and E. K. Lee, *J. Chem. Phys.*, 2014, **141**, 214112.
30 G. Pesce, G. Volpe, G. Volpe and A. Sasso, *Phys. Rev. E*, 2014, **90**, 042309–1–042309–5.
31 T. W. Burkhadart and E. Eisenriegler, *Phys. Rev. Lett.*, 1995, **74**, 3189–3192.
32 J. R. Edison, N. Tasios, S. Belli, R. Evans, R. van Roij and M. Dijkstra, *Phys. Rev. Lett.*, 2015, **114**, 038301.
33 G. D. J. Phillies, *Elementary Lectures in Statistical Mechanics*, Springer, 2000.
34 H. K. Shin, C. Kim, P. Talkner and E. K. Lee, *Chem. Phys.*, 2010, **375**, 316–326.
35 J. M. Varah, *SIAM J. Sci. and Stat. Comput.*, 1983, **4**, 164–176.
36 W. A. Essah and L. M. Delves, *Inverse Problems*, 1988, **4**, 705–724.
37 Z. B. Tsalyuk, *J. Soviet Mathematics*, 1979, **12**, 715–758.
38 Yuhe Ren, Bo Zhang and Hong Qiao, *J. Comput. and Applied Mathematics*, 1999, **110**, 15–24.
39 K. Maleknejad and N. Aghazadeh, *J. Comput. and Applied Mathematics*, 2005, **161**, 915–922.
40 M. Rabbani, K. Maleknejad and N. Aghazadeh, *J. Comput. and Applied Mathematics*, 2007, **187**, 1143–1146.
41 E. H. Hauge and A. Martin-Löf, *J. Stat. Phys.*, 1973, **7**, 259–281.
42 J. L. Lebowitz and P. Résibois, *Phys. Rev.*, 1965, **139**, 1101–1111.
43 R. Zwanzig, *J. Chem. Phys.*, 1964, **40**, 2527–2533.
44 R. Castillo, C. Garza and S. Ramos, *J. Phys. Chem.*, 1994, **98**, 4188–4190.
45 W. C. Swope, H. C. Andersen, P. H. Berens and K. R. Wilson, *J. Chem. Phys.*, 1982, **76**, 637–649.
46 A. Z. Panagiotopoulos, *Mol. Phys.*, 1987, **61**, 813–826.
47 A. Z. Panagiotopoulos, N. Quirke, M. Stapleton and D.J. Tildesley, *Mol. Phys.*, 1988, **63**, 527–545.
48 A. Z. Panagiotopoulos, *Mol. Sim.*, 1992, **9**, 1–23.
49 N. E. Valadez-Perez, A. L. Benavides, E. Schöll-Paschiner and R. Castañeda-Priego, *J. Chem. Phys.*, 2012, **137**, 084905.
50 A. Einstein, *Ann. Phys.*, 1905, **17**, 549.
51 P. Langevin, *C. R. Acad. Sci.*, 1908, **146**, 530.
52 E. Eisenriegler and U. Ritschel, *Phys. Rev. B*, 1995, **51**, 13717–13734.
53 A. Hanke, F. Schlesener, E. Eisenriegler and S. Dietrich, *Phys. Rev. Lett.*, 1995, **81**, 1885–1888.
54 T. F. Mohry, A. Maciolek and S. Dietrich, *J. Chem. Phys.*, 2012, **136**, 224903–1–224903–14.
55 T. F. Mohry, A. Maciolek and S. Dietrich, *J. Chem. Phys*, 2012, **136**, 224902–1–224902–15.
56 J. D. Weeks, D. Chandler and H. C. Andersen, *J. Chem. Phys.*, 1971, **54**, 5237.
57 A. Ahmed and R. J. Sadus, *Phys. Rev. E*, 2009, **80**, 061101–1–061101–9.
58 J. E. Jones, *Proc. R. Soc. Lond. A*, 1924, **106**, 441–462.
59 J. E. Jones, *Proc. R. Soc. Lond. A*, 1924, **106**, 463–477.
60 Loup Verlet, *Phys. Rev.*, 1967, **159**, 98–103.
61 Loup Verlet, *Phys. Rev.*, 1968, **165**, 201–214.
62 D. Levesque and L. Verlet, *Phys. Rev. A*, 1970, **2**, 2514–2528.
63 A. Trokhymchuk and J. Alejandre, *J. Chem. Phys.*, 1999, **111**, 8510–8523.
64 Paul L. Fehder, *J. Chem. Phys.*, 1970, **52**, 791–196.
65 A. Z. Panagiotopoulos, *Observation, prediction and simulation of phase transitions in complex fluids*, NATO ASI Series C Vol. 460, 1995.

66 A. Pelissetto and E. Vicari, *Physics Reports*, 2002, **368**, 549–727.
67 B. J. Alder and T. E. Wainwright, *Phys. Rev. Lett.*, 1967, **18**, 988–990.
68 R. Zwanzig and M. Bixon, *Phys. Rev. A*, 1970, **2**, 2005–2012.
69 F. Sciortino, *Nat. Mater.*, 2002, **1**, 145.
70 A. Scala, M. Reza Sadr-Lahijany, N. Giovambattista, S.V. Buldyrev and H. E. Stanley, *Phys. Rev. E*, 2001, **63**, 041202.
71 J. Kotar, M. Leoni, B. Bassetti, M. C. Lagomarsino and P. Cicuta, *PNAS*, 2010, **107**, 7669.
72 S. Herrera-Velarde, E. C. Euán-Díaz, F. Córdoba-Valdés and R. Castañeda-Priego, *J. Phys.: Conden. Matt.*, 2013, **25**, 325102.